

# Stark effect upon the effective mass and radius in a tight-binding exciton model.

Jean El-khoury\* and Jean-Pierre Gallinar†  
*Departamento de Física, Universidad Simón Bolívar,*  
*Apartado 89000, Caracas 1080A, Venezuela*  
 (Dated: February 1, 2008)

With a Green's function formalism we obtain the eigenvalue spectrum of a tight-binding one-dimensional exciton model characterized by a contact interaction, a Coulombic electron and hole attraction, the Heller-Marcus exciton-hopping energy and an external constant and homogeneous electric field. The resulting eigenvalue spectrum, in the form of an unevenly spaced Wannier-Stark ladder with envelope profiles, is used to obtain the effective mass of the exciton by the application of the Mattis-Gallinar effective mass formula [D. C. Mattis and J.-P. Gallinar, *Phys. Rev. Lett.* **53**, 1391 (1984)]. We obtain positive and negative effective masses for the exciton. The inverse effective mass may oscillate periodically as a function of the inverse of the electric field, with the frequency of oscillation linearly dependent upon the tight-binding hopping matrix element. The exciton radius is also obtained with the Green's function formalism, and it too exhibits Keldysh-like field dependent oscillations, as well as abrupt variations associated to strongly avoided crossings in the eigenvalue spectrum. Finally, some comments are made about the experimental relevance of our results.

PACS numbers: 71.35.-y, 71.35.Cc

## I. INTRODUCTION

As shown by Mattis and Gallinar [1, 2], the mass of an exciton is not, in general, given by the intuitive result of the sum of its electron and hole masses, but it may depend upon excitonic internal quantum numbers, such as, for example, the internal kinetic energy of the exciton [1], or the Heller-Marcus exciton-hopping energy [3]. Beautiful experimental confirmation of some of these surprising, and interesting, predictions, was given by Cafolla et al. [4] in 1985 from electron-energy-loss spectroscopy. Up to now, however, no detailed study or analysis of a specific exciton model [5] has been made [18] in the light of the Mattis-Gallinar formula (MGF) (cf. Eq.(5)) and of its interesting counterintuitive predictions. In view of this, and to further study these predictions, here we shall present a specific, simple, one-dimensional exciton model susceptible to an exact analysis for its eigenvalue spectrum, even while in the presence of an external electric field. Thus enabling the study (in an exact manner) of diverse aspects related not only to the mass of an exciton through the application of the (MGF), but also of those related, for example, to another important general exciton property, such as its radius. As we shall see, some of the shared characteristics of these two exciton parameters (mass and radius) can be understood in terms of the underlying eigenvalue spectrum of the exciton, which, due to the applied external electric field, is obtained to be in the form of an unevenly spaced Wannier-Stark ladder. This ladder, in turn, exhibits Keldysh-like oscillations [6] and strongly avoided crossings of energy levels, with dra-

matic consequences for the mass and radius of the exciton worthy of close examination.

The plan of this paper is then as follows: in Section II we present the mathematical Green's function formalism to be used to obtain the eigenvalue spectrum, as well as the different parameters that go into the exciton model to be considered. In Section III we exhibit a collection of graphical results, and in Section IV conclusions are presented and discussed. Finally, an Appendix with several analytical results is included.

## II. EXCITON MODEL

The one-dimensional exciton model that we will consider [3], akin to that of the Merrifield [7] exciton, can be defined in terms of the matrix elements of the excitonic Hamiltonian  $\mathcal{H}$ . If  $|n, m\rangle$  represents a Wannier orthonormal basis states in which the electron is localized at site  $n$ , and the hole at site  $m$ , the nonvanishing matrix elements of  $\mathcal{H}$  will be taken to be

$$\langle n, m | \mathcal{H} | n, m \rangle = W + V(n - m), \quad (1)$$

where  $W$  represents the combined half-bandwidth of the electron plus hole,  $n - m$  is the relative electron-hole coordinate and  $V(n - m)$  is the effective two-body potential through which the electron and hole interact with each other [7], and with the external electric field, if present [19]. We will assume that  $V(n - m)$  is given by [7]

$$V(n) = -V_o \delta_{n,0} - (1 - \delta_{n,0}) \frac{V}{|n|} + \alpha n, \quad (2)$$

where  $n = 0, \pm 1, \pm 2, \dots$ ,  $V_o$  measures the contact interaction [7], or electron and hole attraction when they are at the same site on top of each other, while, on the

\*Electronic address: elkhoury@ucla.edu

†Electronic address: jpgal@usb.ve

other hand,  $V$  measures the long-range [7] part of the attraction, modelled here by a Coulombic  $1/|n|$  tail. Finally, the interaction of the exciton electric dipole moment with the external electric field  $E$  is given by  $\alpha n$ , with  $\alpha = aeE$ , where “ $a$ ” is the lattice constant and  $(-e)$  the electron charge.

The non-diagonal matrix elements of  $\mathcal{H}$  associated to the kinetic energy of the exciton are given by

$$\begin{aligned}\langle n, m | \mathcal{H} | n, m \pm 1 \rangle &= -t_h, \quad \text{and} \\ \langle n, m | \mathcal{H} | n \pm 1, m \rangle &= -t_e.\end{aligned}\quad (3)$$

With  $t_h$  representing the usual valence-band width parameter associated with nearest-neighbor jumping of the hole, and  $t_e$  the corresponding conduction-band width parameter associated to the electron. Thus,  $W = 2(t_h + t_e)$ . Finally, we introduce the exciton-hopping (or Heller-Marcus) matrix elements given by

$$\langle m, m | \mathcal{H} | n, n \rangle = H(n - m), \quad n \neq m \quad (4)$$

whereby the entire (Frenkel-like) exciton jumps as a whole entity between sites  $n$  and  $m$ , with the amplitude  $H(n - m)$ .

According to the (MGF) [1, 3], the translational mass  $M_n$  of an exciton can be written as

$$M_n = \frac{m_e + m_h}{1 - \frac{K_n}{W} + \frac{m_e + m_h}{M_F} \frac{H_n}{H_F}}, \quad (5)$$

where  $m_e$  and  $m_h$  are, respectively, the electron and hole effective masses,  $K_n$  and  $H_n$  are the expectation values of the kinetic and exciton-hopping energies of the exciton in the  $n$ th bound or localized state of the interaction potential, and, finally,  $M_F$  and  $H_F$  are the values respectively taken by  $M_n$  and  $H_n$  for a Frenkel-like, strongly localized exciton.

As Eq (5) shows, the mass  $M_n$  of the exciton can be determined once the explicit values of  $K_n$  and  $H_n$  are given. These values can be obtained through the Hellmann-Feynman theorem, by writing [3]

$$\begin{aligned}K_n &= \left( \frac{\partial E_n}{\partial \lambda} \right)_{\lambda=\mu=1}, \quad \text{and} \\ H_n &= \left( \frac{\partial E_n}{\partial \mu} \right)_{\lambda=\mu=1};\end{aligned}\quad (6)$$

where  $E_n \equiv E_n(k=0)$  is the eigenvalue of  $\mathcal{H}$  in the  $n$ th bound or localized state of the exciton at  $k=0$ , with  $k$  being the center-of-mass wave vector of the exciton [3]. In Eq. (6),  $E_n$  is made to depend upon the dimensionless parameters  $\lambda$  and  $\mu$  through the following simple scaling [3]

$$t_h \rightarrow \lambda t_h$$

$$t_e \rightarrow \lambda t_e,$$

and

$$H(n - m) \rightarrow \mu H(n - m). \quad (7)$$

A Green's function formalism [8, 9] permits then the evaluation [3] of the energy eigenvalues  $E_n$ , by finding the simple poles  $z_n(m)$  of the continued fraction  $G_{m,m}(z)$  given by

$$\begin{aligned}G_{m,m}^{-1}(z) &= z - V(m) - \frac{\varepsilon^2}{z - V(m+1) - \cdots} \\ &\quad - \frac{\varepsilon^2}{z - V(m-1) - \cdots}.\end{aligned}\quad (8)$$

Where  $\varepsilon = \lambda(t_e + t_h)$ , and  $m = 0, \pm 1, \pm 2, \dots$  is a fixed integer. Due to the peculiar nature of the Heller-Marcus [20] exciton-hopping energy [3], the Term  $V(0)$  appearing in Eq. (8) is shifted so that [3]  $V(0) \rightarrow V(0) + \mu H_F$ . The set of all eigenvalues  $E_n$  of  $\mathcal{H}$  can then be found and ordered appropriately [9] from the relationships  $E_n = z_n(m) + W$ , in a manner over-all independent of the chosen  $m$ 's (from now on for simplicity we write  $z_n(m) \equiv z_n$ ).

The mean-square radius  $R_n^2$  of the exciton can also be found in terms of  $G_{m,m}^{-1}(z)$ . In fact, the mean-square radius of the exciton is defined in terms of the relative electron-hole coordinate  $m$ , as

$$R_n^2 = \sum_{m=-\infty}^{m=+\infty} a^2 m^2 |F_n(m)|^2, \quad (9)$$

where  $F_n(m)$  is the normalized relative coordinate wavefunction of the exciton [3]. As shown in the Appendix, the Green's function formalism [9] permits then the direct evaluation of  $|F_n(m)|^2$ , obtaining finally

$$R_n^2 = \sum_{m=-\infty}^{m=+\infty} \frac{a^2 m^2}{\left( \frac{\partial}{\partial z} G_{m,m}^{-1}(z) \right)_{z=z_n}}. \quad (10)$$

In contrast with the evaluation of the set of eigenvalues  $E_n$ , all values of  $m$  are seen in Eq (10) to be in principle relevant for the evaluation of  $R_n^2$ . In the next section 3 we shall display some of the results obtained through the use of the above described formalism applied to our exciton model.

### III. RESULTS

In this section we display three types of results: energy spectra, effective masses and root-mean-square radii of the exciton. Figures (1) and (2) were obtained starting from the numerical evaluation [10] of the continued fraction in Eq.(8). In Fig (1),  $m$  was chosen for evaluation purposes as  $m=0$  due to absence of Coulomb interaction, while in Fig (2)  $m$ 's different from zero were appropriately chosen for ease of computation. Because of

the contact interaction  $V_o$  being  $V_o/\alpha = 10$ , level  $n = 0$  in the ladder in Fig (1) is moved down to the level  $n = -10$  where a degeneracy occurs at  $t = 0$ . While in Fig (2), with Coulomb interaction, no such degeneracy occurs for the selected parameters. In both Figures (1) and (2), several (strongly) avoided energy crossings are evident and are associated to the envelope profiles. In Fig (1), the envelope profile which starts at  $z_n/\alpha = -10$  is that of the single bound state [11] of the contact interaction  $V_o$  (in absence of the electric field), i.e.,

$$E_n - W = -\sqrt{V_o^2 + W^2}. \quad (11)$$

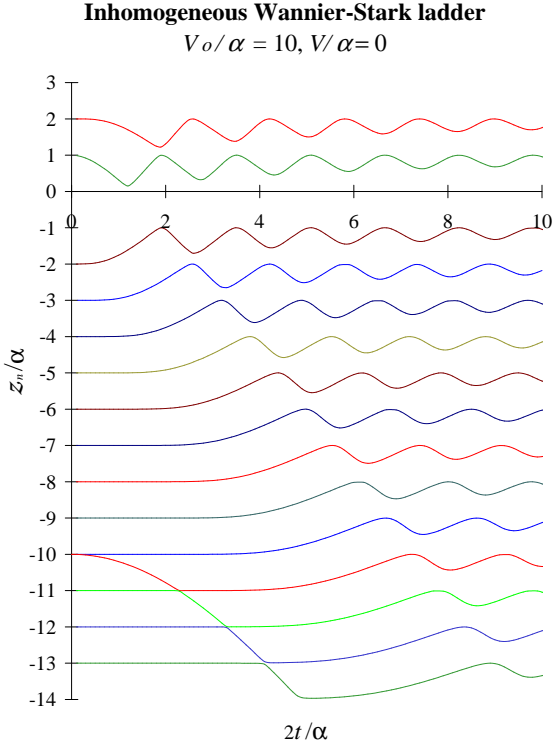


FIG. 1: Inhomogeneous Wannier-Stark Ladder energy levels  $E_n - W$  for the exciton in terms of  $z_n(m)/\alpha$  vs  $2t/\alpha$ , with  $V = 0$  and  $V_o/\alpha = 10$ ;  $n$  runs from  $-13$  to  $2$  (skipping  $n = -1$  for visual convenience), the chosen  $m$  is zero and henceforth  $t \equiv t_e = t_h$ . Note the increment in the degree of flatness down in the ladder where a large number of derivatives is identically zero at  $t = 0$ . Noteworthy characteristics of the ladder are: oscillations as  $t$  increases, strongly avoided energy crossings and envelope profiles. Energy levels  $n = 0$  and  $n = -10$  are degenerate at  $t = 0$ .

As for Fig (3), it was numerically obtained using a scaling property [1] (valid when  $H_F = 0$ ) related to the energy  $E_n(k; t)$ , namely,

$$E_n(k; t) - W = z_n(k; t) = z_n(0; t \cos ka). \quad (12)$$

Different exciton masses are to be associated to levels  $n = 0$  and  $n = -10$ , which have respective curvatures of different magnitude at  $k = 0$  in Fig (3).

### Inhomogeneous Wannier-Stark ladder $V_o/V=3, V_o/\alpha=10$

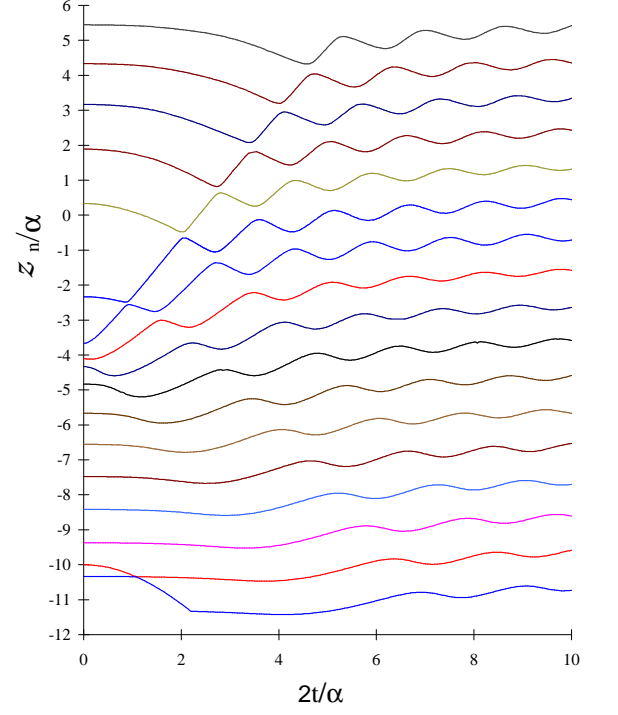


FIG. 2: Inhomogeneous Wannier-Stark Ladder energy levels  $E_n - W$  for the exciton in terms of  $z_n(m)/\alpha$  vs  $2t/\alpha$ , with  $V_o/V = 3$  and  $V_o/\alpha = 10$ ;  $n$  runs from  $-10$  to  $6$ , the chosen  $m$ 's are not all zero and  $t \equiv t_e = t_h$ . Note the increment in the degree of flatness down in the ladder where a large number of derivatives is vanishingly small at  $t = 0$ . Noteworthy characteristics of the ladder are: oscillations as  $t$  increases, strongly avoided energy crossings and envelope profiles.

Figures (4), (5) and (6) display a small representative sample of our results for the effective exciton mass  $M_n$  [12]. Interestingly enough, we find both positive and negative effective masses with  $|\frac{m_e + m_h}{M_n}| \leq 1$  when  $M_F = \infty$  (i.e., in absence of the Heller-Marcus effect in Figures (4) and (5)). In Fig 6 we find that the exciton-hopping effect [3] shifts the mass away from negative values but still allows for effective negative masses. That the effective mass of the exciton may indeed become negative in the presence of an external electric field is an interesting result found here that has not been properly noted [13] in the previous literature [1, 2, 3, 5], and might be of experimental relevance for the excitonic Stark effect. The noticeable visual envelope for the inverse mass in Fig (4) arises from the bound state of Eq.(11), or envelope

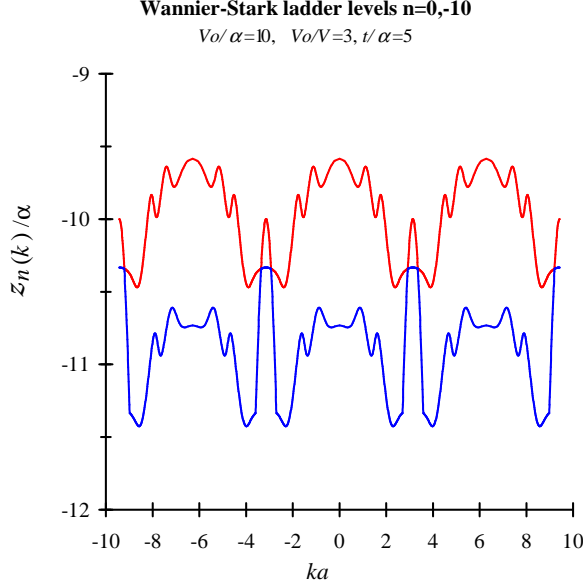


FIG. 3: Plot of Wannier-Stark ladder levels  $n = 0$  (red) and  $n = -10$  (blue) vs  $ka$  in the first three Brillouin Zones. The strongly avoided crossing of corresponding levels shown in figure 2 appears here close to the borders of the Brillouin Zones.

profile of Fig (1). It is given by [11]

$$\left( \frac{m_e + m_h}{M_n} \right)_{env.} = \frac{x}{\sqrt{1 + x^2}}, \quad (13)$$

where  $x \equiv W/V_o$ .

In Figures (5) and (6), the inverse of the mass is seen to oscillate (for  $\alpha^{-1} \rightarrow \infty$ ) as a function of  $1/\alpha$ . The period  $P$  of these Keldysh-like oscillations can be shown to be (see Appendix)

$$P = \frac{\pi}{4} \left( \frac{V_o}{t} \right). \quad (14)$$

Numerical results [12] furthermore show Eq.(14) to be still valid when the Coulomb interaction  $V$  is present, i.e., the period of these oscillations is independent of  $V$ .

Our three remaining figures display typical behavior of the root-mean-square radius  $R_n$  of the exciton in our model. Figures (7) and (8) display an oscillatory behavior as  $R_n$  diverges with increasing  $t \rightarrow \infty$ . Superimposed on both figures (7) and (8) is an overall hyperbolic “pattern”, given by the formula (see Appendix)

$$\frac{R_n}{a} = \sqrt{\frac{8t^2}{\alpha^2} + n^2}, \quad (15)$$

which expresses the value of  $R_n$  under the action of the electric field alone, i.e., for a homogenous equally spaced Wannier-Stark ladder, with eigenvalues  $E_n - W = n\alpha$ .

In Fig.(8) the radius  $R_n/a$  for  $n = 0$  starts at zero, and for small enough  $2t/\alpha$  it increases linearly (cf. Eq.(15))

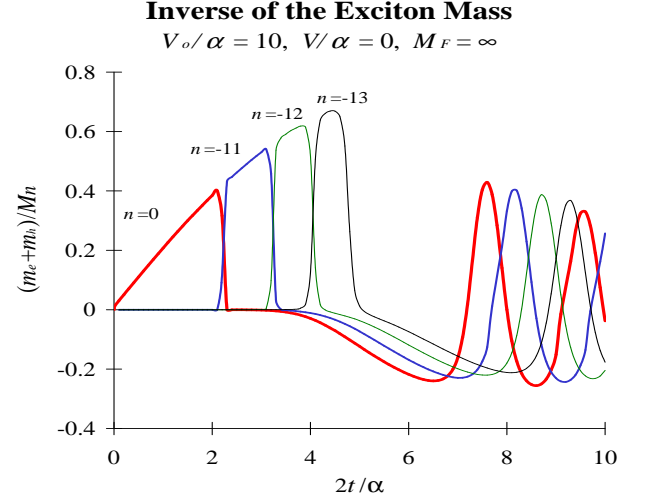


FIG. 4: Plot of the inverse effective dimensionless mass  $(m_e + m_h)/M_n$  vs  $2t/\alpha$ , with  $V_o/\alpha = 10$  and  $M_F = \infty$ , for the energy levels  $n = 0, -11, -12, -13$ . Both here and in the Wannier-Stark ladder in figure 1, these levels give rise to a noticeable visual envelope and abrupt changes in the exciton mass. The amplitude of the oscillations decreases for large values of  $2t/\alpha$ .

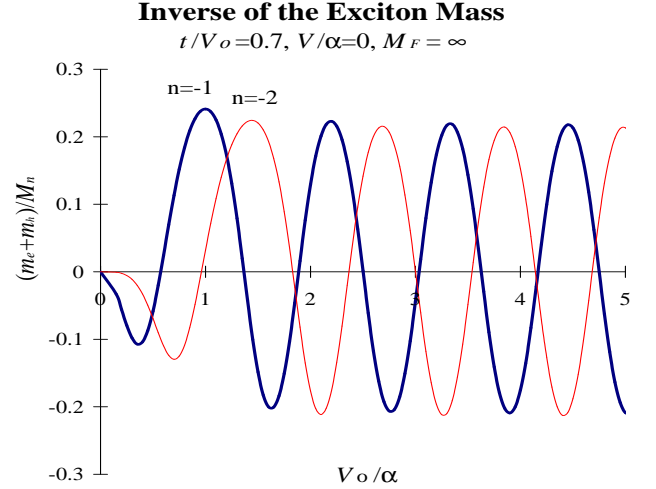


FIG. 5: Plot of the inverse effective dimensionless mass  $(m_e + m_h)/M_n$  vs  $V_o/\alpha$ , with  $t/V_o = 0.7$ ,  $V/V_o = 0$  and  $M_F = \infty$ , for two energy levels ( $n = -1, -2$ ) from the Wannier-Stark Ladder in figure 1. As  $\alpha^{-1} \rightarrow \infty$ , the curves become periodic in the inverse electric field  $1/\alpha$ , with period  $P$  given by  $P = \frac{\pi}{4} (V_o/t) \approx 1.122$ .

until it reaches the value of  $2t/\alpha \sim 1$ . At this point one observes an abrupt variation of  $R_n/\alpha$  for both levels ( $n=0, -10$ ), and a simultaneous strongly avoided crossing in the Wannier-Stark ladder. From then on the contribution to the linear increase in the radius (cf. Fig.(2)) is given by the following level down in the Wannier-

**Inverse of the Exciton mass**  
 $n = -2$ ,  $t/(V_o - H_F) = 0.2$ ,  $V/V_o = 0$

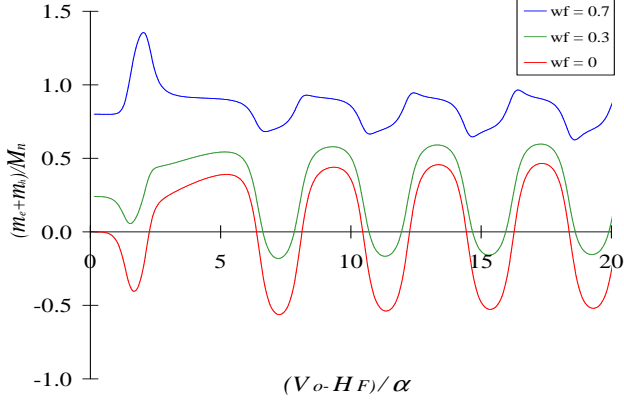


FIG. 6: Plot of the inverse effective dimensionless mass  $(m_e + m_h)/M_n$  vs  $V_o/\alpha$  for the energy level  $n = -2$ , with  $t/V_o = 0.2$ ,  $V/V_o = 0$ , and three values of the Wannier-Frenkel ratio  $(m_e + m_h)/M_F \equiv wf$ . The Heller Marcus effect shifts the mass away from negative values. As  $\alpha^{-1} \rightarrow \infty$ , the curves become periodic in the inverse electric field  $1/\alpha$ , with identical period  $P$  given by  $P = \frac{\pi}{4}(V_o - H_F)/t \approx 3.927$ .

**Exciton Radius**  
 $V_o/\alpha = 10$ ,  $V_o/V = 3$

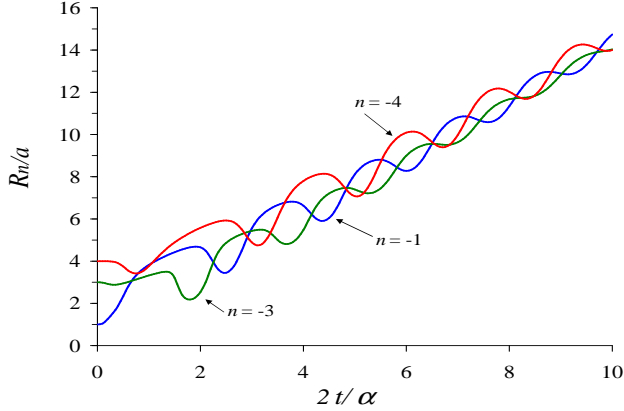


FIG. 7: Plot of the dimensionless exciton radius  $R_n/a$  vs  $2t/\alpha$  for three levels ( $n = -1, -3, -4$ ), with  $V_o/\alpha = 10$  and  $V_o/V = 3$ . At  $t = 0$  exciton motion is frozen, with expected inter-particle distance equal to  $|n|$ . As  $t \rightarrow \infty$  exciton radius diverges in an oscillatory manner.

Stark ladder (here  $n=-10$ ). These abrupt variations in the exciton's size, exemplified here with these two levels ( $n = 0, -10$ ), are, however, a general feature of our model [12]. One which will always occur associated to a strongly avoided crossing in the respective eigenvalue spectrum, and one which has no counterpart in the study of, for example, the standard Stark effect for the hydro-

**Exciton Radius**  
 $V_o/\alpha = 10$ ,  $V_o/V = 3$

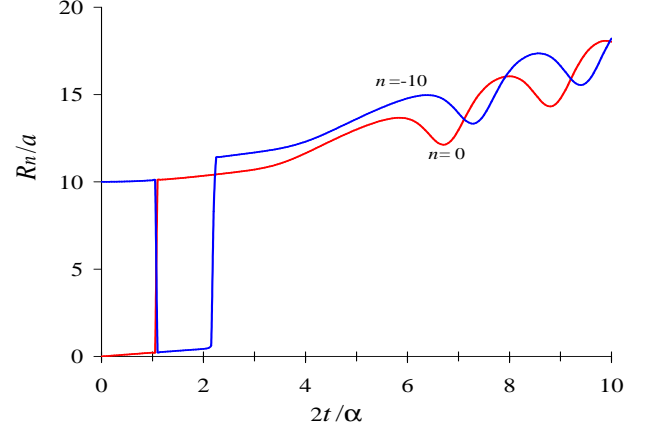


FIG. 8: Plot of the dimensionless exciton radius  $R_n/a$  vs  $2t/\alpha$  for two levels  $n = 0$  (red) and  $n = -10$  (blue), with  $V_o/\alpha = 10$  and  $V_o/V = 3$ . The exciton radius shows abrupt variations due to the strongly avoided crossings in the corresponding energy spectrum (figure 2). Note the envelope associated to each one of the exciton radii, arising from the envelope in the Wannier-Stark ladder.

**Exciton Radius**  
 $V_o/\alpha = 10$ ,  $V_o/V = 3$ ,  $t/\alpha = 5$

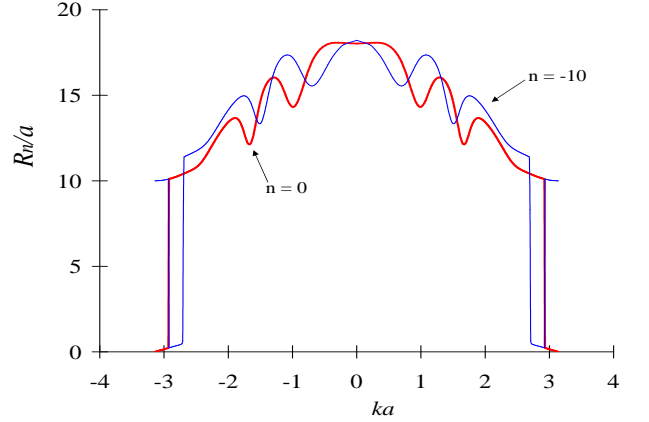


FIG. 9: Plot of the dimensionless exciton radii  $R_n/a$  for  $n = 0$  (red) and  $n = -10$  (blue) vs  $ka$  in the first Brillouin Zone. The strongly avoided crossing of corresponding levels shown in figure 2 appears here as abrupt variations of the radii close to the borders of the first Brillouin Zone.

gen atom [6].

Finally, in Fig. (9) we display the  $k$ -dependence of  $R_n/a$  for the same levels as in Fig.(8) at  $t/\alpha = 5$ . The abrupt variations in Fig. (8) are displayed in Fig. (9) close to the first Brillouin Zone borders, and oscillations of  $R_n/a$  in one curve are transposed onto the other.

Having displayed graphically some of our extensive [12] numerical results, in the next section some conclusions

are presented and comments made about the relevance of our exciton model.

#### IV. CONCLUSIONS

Although simple, the exciton model considered previously displays quite interesting behavior. Most notably, oscillating (negative) excitonic masses and abrupt variations in the exciton's size (among others). To the best of our knowledge, these are novel predictions that have not been considered before in the literature, nor have these effects been experimentally observed. Since the strongly ionizing influence of an external electric field upon a weakly bound exciton is well-known [13], it is clear that the difficulty of experimental observation of some of these effects might be a large one. Furthermore, it is unclear to what extent the previous theoretical results may be modified by, for example, the inclusion of a more realistic exciton (band) dispersion law, as well as the lifting of the one-dimensionality of the model. To this extent, further investigation of our model's interesting predictions is warranted in the future.

From a self-consistent point of view it is worthwhile to point out that, within the context of the model's given tight-binding dispersion, the semiclassical effective potential [14]  $V_{eff.}(n)$  associated to  $V(n)$  (cf. Eq. (2)), is given by [15]

$$V_{eff.}(n) = \mu^* \left[ \frac{a^2}{2} V^2(n) - a^2 \mathbf{E} V(n) \right], \quad (16)$$

(where  $\mathbf{E}$  is the semiclassical energy of the exciton and  $\mu^*$  is the reduced mass of the electron and hole). Since  $V_{eff.}(n)$  is positive and diverges for  $|n| \rightarrow \infty$ , this precludes the occurrence of the well-known [13] tunneling through the potential barrier that appears in the standard Stark effect for the hydrogen atom, or for a non tight-binding exciton in the parabolic effective mass approximation [13]. Thus, our bound exciton states on the lattice are truly localized [16], instead of being simply metastable ones as for a hydrogen-like atom on the continuous manifold [21], and consequently, both the mass and the radius of the exciton are well-defined concepts for these states. It is to be noticed, finally, that although presented in the context of the (MGF), our exact results for the effective mass  $M_n$  of the exciton have also been obtained independently [12] from the exciton dispersion law  $E_n(k)$ . Thus the validity of the (MGF) has in this respect also been checked.

In summary, we have considered a very simple one-dimensional exciton model in the presence of a static and homogenous electric field, and this model has been found to display highly interesting behavior for some of its properties, such as mass and radius [22]. Further theoretical work should then be able to elucidate to what extent some of these predicted effects might be experimentally observable.

#### APPENDIX

In this Appendix we derive several analytical results used in this paper. First, we obtain Eq.(10) in the text from the definition in Eq.(9). Based on the Green's function formalism [9], the continued fraction  $G_{m,m}(z)$  can be written as:

$$G_{m,m}(z) = \sum_{m'} \frac{|F_{m'}(m)|^2}{z - z_{m'}}. \quad (A.1)$$

where the  $z_{m'}$ 's are simple poles of  $G_{m,m}(z)$ . Multiplying both sides of Eq. (A.1) by  $(z - z_n)$ , we obtain:

$$(z - z_n) G_{m,m}(z) = \sum_{m'} \frac{z - z_n}{z - z_{m'}} |F_{m'}(m)|^2, \quad (A.2)$$

and by taking the limit ( $z \rightarrow z_n$ ), we get

$$\lim_{z \rightarrow z_n} (z - z_n) G_{m,m}(z) = |F_n(m)|^2, \quad (A.3)$$

or equivalently

$$\lim_{z \rightarrow z_n} \frac{(z - z_n)}{G_{m,m}^{-1}(z)} = \frac{1}{\frac{\partial}{\partial z} (G_{m,m}^{-1}(z))_{z=z_n}} = |F_n(m)|^2. \quad (A.4)$$

By substituting the result of Eq.(A.4) into Eq.(9) we obtain Eq.(10).

Now we obtain Eq.(14) which gives the period  $P$  of the Keldysh-like oscillations observed in the energy and the inverse mass of the exciton in the limit  $t/\alpha \rightarrow \infty$ . On one hand, we start with Eq.(8) written in the absence of the Coulomb interaction, i.e., with  $V(m) = -V_o \delta_{m,0} + \alpha m$  [23], and then we use the following relationship

$$\frac{y}{2\nu} \frac{J_{\nu-1}(y)}{J_\nu(y)} - 1 = \frac{-\frac{\left(\frac{y}{2}\right)^2}{\nu(\nu+1)}}{1 - \frac{\frac{\left(\frac{y}{2}\right)^2}{(\nu+1)(\nu+2)}}{1 - \frac{\frac{\left(\frac{y}{2}\right)^2}{(\nu+2)(\nu+3)}}{1 - \ddots}}}, \quad (A.5)$$

which expresses Bessel functions  $J_\nu(y)$  of the first kind in a continued fraction form [17]. Using the following identities

$$J_{\nu+1}(y)J_{-\nu}(y) + J_\nu(y)J_{-\nu-1}(y) = \frac{-2 \sin(\nu\pi)}{\pi y},$$

$$J_{\nu-1}(y) + J_{\nu+1}(y) = \frac{2\nu}{y} J_\nu(y), \quad \text{and} \quad (A.6)$$

$$J_\nu(-y) = (-1)^\nu J_\nu(y), \quad (A.7)$$

Eq. (8) can then be written (for  $m = 0$  and  $\varepsilon \equiv 2t$ ) as

$$G_{0,0}^{-1}(z) = \frac{\alpha}{\pi} \frac{\text{sen}(\nu\pi)}{J_\nu(y)J_{-\nu}(y)} - V_o, \quad (\text{A.8})$$

where  $\nu \equiv z/\alpha$  and  $y \equiv 4t/\alpha$ .

The eigenvalues  $E_n$  are obtained from the following implicit equation upon the  $z_n$ 's, namely

$$\sin\left(\frac{z_n}{\alpha}\pi\right) = \left(\frac{V_o\pi}{\alpha}\right) J_{\frac{z_n}{\alpha}}\left(\frac{4t}{\alpha}\right) J_{-\frac{z_n}{\alpha}}\left(\frac{4t}{\alpha}\right), \quad (\text{A.9})$$

obtained in turn from  $G_{0,0}^{-1}(z) = 0$ . When  $\alpha^{-1} \rightarrow \infty$ , we use the asymptotic Bessel functions form [17]

$$\lim_{y \rightarrow \infty} J_{\pm\nu}(y) = \sqrt{\frac{2}{\pi y}} \cos\left(y \mp \frac{1}{2}\nu\pi - \frac{1}{4}\pi\right). \quad (\text{A.10})$$

Upon substitution of Eq.(A.10) into Eq.(A.9), we obtain after some algebraic manipulations that

$$\begin{aligned} \frac{4t}{V_o} \sin\left(\frac{z_n}{\alpha}\pi\right) &= \cos^2\left(\frac{1}{2}\frac{z_n}{\alpha}\pi\right) - \sin^2\left(\frac{1}{2}\frac{z_n}{\alpha}\pi\right) \\ &\quad + 2 \sin\left(\frac{4t}{\alpha}\right) \cos\left(\frac{4t}{\alpha}\right), \text{ or} \\ \frac{4}{A} \sin\left(\frac{z_n}{\alpha}\pi\right) &= \cos\left(\frac{z_n}{\alpha}\pi\right) + \sin\left(\frac{8}{A}\frac{V_o}{\alpha}\right); \end{aligned} \quad (\text{A.11})$$

$z_n/\alpha$  as a function of  $V_o/\alpha$  will then be periodic with period  $P = \frac{\pi}{4}A$ , where  $A \equiv \frac{V_o}{t}$ , and so will the inverse mass of the exciton according to Eq.(5).

To end this Appendix we indicate briefly the derivation of Eq.(15). By setting  $V_o = V = H_F = 0$  in Eq. (8), we find

$$G_{m,m}^{-1}(z) = \frac{(-1)^m \frac{\alpha}{\pi} \sin\left(\frac{z}{\alpha}\pi\right)}{J_{\frac{z}{\alpha}-m}\left(\frac{4t}{\alpha}\right) J_{-\frac{z}{\alpha}+m}\left(\frac{4t}{\alpha}\right)}, \quad (\text{A.12})$$

which can be proven [12] in a manner analogous to that of Eq. (A.8). One now evaluates the derivative of  $G_{m,m}^{-1}(z)$  appearing in Eq. (10), as

$$\frac{\partial}{\partial z} G_{m,m}^{-1}(z)|_{z=z_n} = \frac{(-1)^{n+m}}{J_{n-m}\left(\frac{4t}{\alpha}\right) J_{-n+m}\left(\frac{4t}{\alpha}\right)}, \quad (\text{A.13})$$

where  $z_n = n\alpha$ . Substituting Eq. (A.13) into Eq. (10), there results

$$R_n^2 = \sum_{m=-\infty}^{m=+\infty} (-1)^{m+n} a^2 m^2 J_{(n-m)}\left(\frac{4t}{\alpha}\right) J_{-(n-m)}\left(\frac{4t}{\alpha}\right), \quad (\text{A.14})$$

which reduces to

$$\frac{R_n^2}{a^2} = \sum_{m=-\infty}^{m=+\infty} m^2 J_{n+m}^2\left(\frac{4t}{\alpha}\right), \quad (\text{A.15})$$

by using Eq. (A.7). Eq. (15) finally ensues after some algebraic manipulations [12] on Eq. (A.15)

- 
- [1] D. C. Mattis and J.-P. Gallinar, *Phys. Rev. Lett.* **53**, 1391 (1984).
  - [2] D. C. Mattis, *Rev. Mod. Phys.* **58**, 361 (1986).
  - [3] J.-P. Gallinar and D. C. Mattis, *Phys. Rev. B* **32**, 4914 (1985).
  - [4] A. A. Cafolla, S. E. Schnatterly, and C. Tarrio, *Phys. Rev. Lett.* **55**, 2818 (1985).
  - [5] J.-P. Gallinar, *J. Phys.: Condens. Matter* **8**, 3103 (1996), and references therein.
  - [6] J. Callaway, *Quantum Theory of the Solid State* (Academic Press, New York, 1974).
  - [7] R. E. Merrifield, *J. Chem. Phys.* **34**, 1835 (1961).
  - [8] J.-P. Gallinar, *Phys. Lett.* **103A**, 72 (1984).
  - [9] E. N. Economou, *Green's functions in Quantum Physics*, Springer Series in Solid-State Sciences 7 (Springer-Verlag, Berlin, 1979).
  - [10] W. Press, S. A. Teukolsky, W. T. Vetterling, and B. P. Flannery, *Numerical Recipes: The Art of Scientific Computing* (Cambridge University Press, New York, 1986).
  - [11] J.-P. Gallinar, *Phys. Rev. B* **36**, 1782 (1987).
  - [12] J. El-khoury, Master's thesis, Universidad Simón Bolívar, Venezuela (1999), available upon request at elkhoury@ucla.edu.
  - [13] E. I. Rashba, *Excitons* (North-Holland, Amsterdam, 1982), edited by E. I. Rashba and M. D. Sturge.
  - [14] N. W. Aschcroft and N. D. Mermin, *Solid State Physics* (Holt, Rinehart & Winston, New York, 1976).
  - [15] J.-P. Gallinar and J. El-khoury (2001), unpublished.
  - [16] S. I. Serdyukova and B. N. Zakhariev, *Phys. Rev. A* **46**, 58 (1992).
  - [17] *Handbook of Mathematical Functions* (Dover, New York, 1965), edited by M. Abramowitz and I. A. Stegun.
  - [18] With or without an externally applied electric field.
  - [19] No external field is considered in [7].
  - [20] The Heller-Marcus term acts only when the electron and hole are at the same lattice site.
  - [21] Furthermore, our Green's function matrix elements  $G_{m,m}(z)$  have no cuts, i.e., they display only isolated poles on the real axis.
  - [22] Largely independent of boundary conditions, since it is noteworthy that placing our system in a finite "box" (so as to make the limit  $\alpha \rightarrow 0$  non-singular) does not alter significantly any of our physical results [12].
  - [23] When there is exciton-hopping,  $V_o$  is simply replaced by  $V_o - H_F$